Design and fabrication of a hybrid nanofluidic channel

Gary J. Cheng
Daniel Pirzada
Prashanta Dutta
Washington State University
School of Mechanical
and Materials Engineering
Pullman, Washington 99164
E-mail: dutta@mail.wsu.edu

Abstract. A hybrid micro-nanofluidic channel network is developed on a silicon wafer for bioanalytical applications, such as separation, concentration, and fractionation. The nanochannel is formed on the silicon wafer using surface micromachining techniques, while the microchannel is fabricated on the poly-di-methyl-siloxane utilizing soft lithography techniques. Microfluidic networks not only support the very thin wall of the nanofluidic channel, but also provide appropriate gateways for the fluid/sample flow. The thickness of the microchannels is kept below 10 μm by changing the spin rate and time during photolithography. On the other hand, nanochannel thickness is varied between 100 and 200 nm by controlling the sputtering time of the sacrificial copper layer. Electrochemical wet etching is employed to release the thin layer of copper from the silicon dioxide shell. Our etching technique demonstrates significant advantages over other existing methods, such as wet chemical etching and reactive ion etching, including relatively fast etching rate, good selectivity, less safety and environmental concerns, less monitoring and control issues, and low cost. The dimensions of our microfluidic channels are measured using a profilometer, while the nanochannel thickness is confirmed by the atomic force microscopy and scanning electron microscopy images.
[DOI: 10.1117/1.1869132]

Subject terms: nanofluidic; electrochemical etching; poly-di-methyl-siloxane; hybrid channel.

Paper 04033 received Jun. 10, 2004; revised manuscript received Aug. 16, 2004; accepted for publication Aug. 24, 2004; published online Mar. 4, 2005.

1 Introduction

Research and development on chemical transport phenomena in micro- and nanofluidic channel networks have been a frontier in fluid dynamics[1–4] in the past decade. Micro- and nanofluidic systems have been applied in separation of molecules, manipulation and detection of individual biomolecules,[5–8] etc. The validation of theoretical and simulation studies on some unique transport properties[1,9,10] has been hindered because of the lack of available functional nanofluidic systems. It is crucial that fabrication techniques for nanofluidic systems enable nanoscale patterning, be able to integrate with micro- and mesoscale components, be flexible in design, be biocompatible with molecules, and be amenable to mass production.

Fabrications of nanoscale devices and systems have been extensively investigated recently, and e-beam lithography has been most widely used in producing nanofluidic systems with controlled feature in nanoscale. Moreover, e-beam lithography enables complex patterning in nanoscale.[11,12] However, mass production is not feasible with e-beam lithography due to its serial processing nature. It is also not useful for producing large areas of nanostructures. Nanoimprint lithography has been proposed as an alternative approach to solve these problems.[7,13,14] In nanoimprint, a mold is fabricated first with e-beam lithography for nanoscale features[14,15] and optical lithography for larger features. The molded pattern is then transferred to a thermoplastic polymer through heat and pressure or into a UV polymerizing liquid.[16] Nanoimprint lithography approaches are parallel, suitable for nanoscale patterns over macroscopic areas. However, fabrication is not flexible because a new mold must be made whenever there is a change in the nanofluidic features. The wearing of the mold also poses a challenge to mass production.

Stern et al.,[17] fabricated nanocapillary channels with heights between 20 and 100 nm using a combination of integrated circuit processing and differential etching techniques. These channels were proposed for a very sensitive chemical sensor, the chemical charge-coupled device (CCCD). In this technique, the etching of the sacrificial layer takes 60 to 80 h for a 2-mm-long channel. Their technique not only takes an extremely long etching time, but also the structural material of the channel, Si_3N_4, is etched with the sacrificial layer, amorphous Si. This causes thinning of the dielectric layer and impacts the interfacial quality of the dielectric-electrolyte interface. Generally crack, peel, and collapse occur as soon as amorphous Si is removed. Moreover, the structural integrity is degraded significantly when channel width is greater than 30 μm.

O'Brien et al.,[18] created functional nanofluidic channels with feature sizes ranging from 100 nm to 2 mm based on an all-optical lithographic process and wafer bonding. Interferometric lithography, a maskless technique based on the interference of two or more coherent beams, was used to inexpensively and quickly pattern nanoscopic features

1537-1646/2005/$22.00 © 2005 SPIE

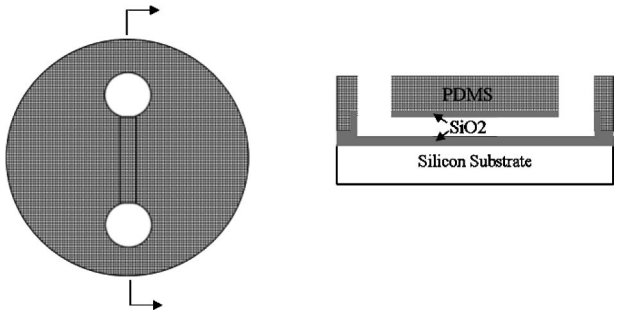

Fig. 1 Schematic top and cross-sectional views of a hybrid PDMS-SiO_2 nanofluidic channel.

over large surface areas with easily varied feature dimensions, pitch size, and channel width. It is well suited to high-throughput manufacturing. However, this method must use interferometric lithography, which is expensive and not available in many clean rooms. Also, in their technique, the width of the channel is limited by the etching depth of dry etching, which is no more than a few micrometers for a nanochannel. The aspect ratio of the channel is also limited by dry etching, which often results in a tapered-shape cross-sectional nanofluidic channel.

Most recently, Guo et al.[19] developed a nanofabrication technique to make periodic nanochannels. In that work, nanoscale channel manifolds were first created using nanoimprint lithography and reactive ion dry etching techniques, and then the channel templates were used to form nanochannels by displacing a very thin layer of polymeric materials. However, this process must fabricate a nanoscale protrusion, which requires nanoimprint lithography and is not available in many microfabrication facilities. Also, once a mold is formed, it is not flexible to change the geometry of the channel.

In this paper, we describe a nanochannel fabrication technique that is easily implemented in clean rooms without dry etching and e-beam lithography. This fabrication process combines surface micromachining, wafer bonding, and electrochemical etching. The channel width is varied between 5 and 300 μm, which is determined by UV lithography. The channel height is determined by the thickness of a sputtered Cu layer, which is deposited and then removed as sacrificial layer. The etching of the nanoscale sacrificial layer is implemented by electrochemical etching to significantly reduce fabrication time. The fabricated nanochannel is bonded with poly-di-methyl-siloxane (PDMS) before releasing the sacrificial copper layer so that structural integrity is maintained, and no peel or collapse occurs.

2 Fabrication, Integration, and Measurement

2.1 *Fabrication of Nanochannel*

Schematic top and cross-sectional views of a hybrid PDMS-SiO_2 nanofluidic channel are shown in Fig. 1. The device fabrication steps for the hybrid nanochannel are outlined in Fig. 2. Silicon $\langle 100 \rangle$ wafers were cleaned in piranha solution (H_2O_2:H_2SO_4=1:2 in volume), triple rinsed with deionized (DI) water, dipped in HF acid to remove the native oxide layer and any remaining inorganic contaminants, and then triple rinsed with DI water again. The silicon substrate was wet oxidized to form a 1-μm SiO_2 layer. Using humidified oxygen as the carrier, the wet oxidation was conducted by maintaining an oxygen pressure of 5 psi and a flow rate of 6 ml/min. The oxygen gas was humidified by bubbling the oxygen through DI water at 95 °C. The oxidation was conducted at 1050 °C for 60 min, which resulted in a SiO_2 film thickness of 1 μm.

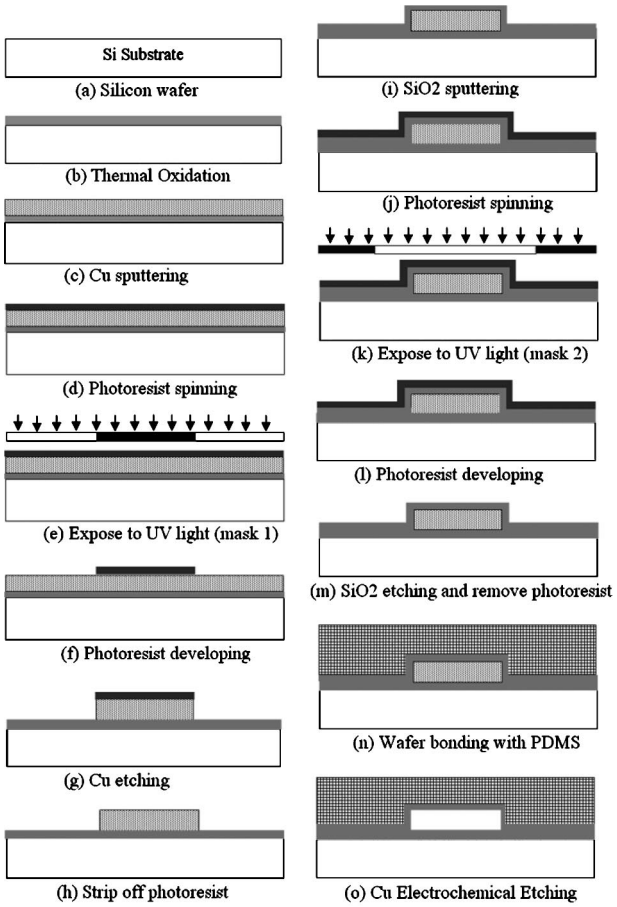

Fig. 2 Schematic views of the fabrication process of a nanochannel on a silicon substrate.

The next step is to deposit a sacrificial 100- to 200-nm-thick layer on the SiO_2 layer. Copper was chosen as the sacrificial material because of the proposed electrochemical etching and the convenience of sputtering a Cu thin film on SiO_2. Here a copper film of 100 to 200 nm was deposited by sputtering (step c) using Edwards Sputter-System Auto 306. The sputtering was performed in radio frequency (rf) mode for 20 to 40 s at 275 V and 100 W under a process pressure of 3×10^{-3} Torr. The flow rate of argon was 2 ml/min during sputtering.

After sputtering, the Cu thin film was patterned and selectively etched to form the shape of a nanochannel. The lithography and patterning were done using photoresist and mask aligner (HYBRALIGN-500). After being spin-coated with photoresist AZ5214, each sample was hard baked at 170 °C for 3 min (step d). The wafer was then exposed to UV laser (step e) using the mask file shown in Fig. 3 (mask 1). After exposure, the photoresist was developed (step f) using undiluted MF702 developer (Shipley, Inc.) and rinsed

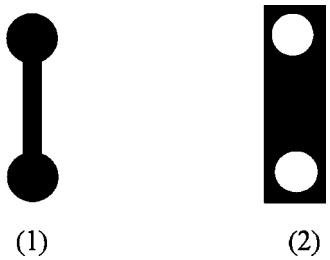

Fig. 3 Masks 1 and 2 for the nanochannel fabrication.

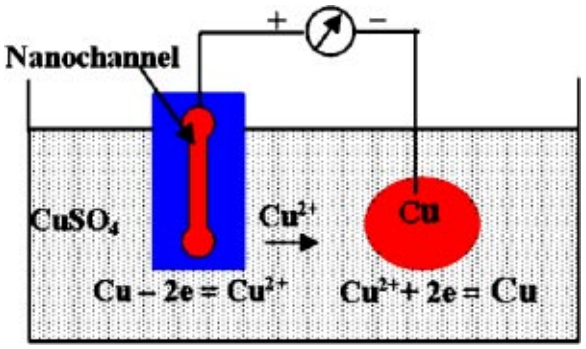

Fig. 4 Schematic view of the electrochemical etching of copper to form the nanochannel.

with DI water. The exposed Cu was then etched with diluted H_2SO_4 (step g). The remaining photoresist was stripped off with acetone. In our fabrication process, the channel manifold was 300 μm in width and 20 mm in length.

Next a SiO_2 thin layer of 1 μm was deposited on top of the Cu using the sputtering technique (step i). The SiO_2 was also sputtered in rf mode at 275 V and 75 W for 20 min under an argon pressure of 2.5×10^{-3} Torr and argon flow of 2 l/min. The SiO_2 film thickness was measured with an SPN profilometer to be 1 μm.

Two holes were then opened at the end of the nanochannel to connect the nanochannel with external micro- and/or mesofluidic systems. The lithography and patterning of the two holes were done with photoresist and UV mask aligner. After being spin-coated with photoresist AZ5214, each sample was hard baked at 170 °C for 3 min (step j). The wafer was then exposed to UV light (step k) using the mask file shown in Fig. 3 (mask 2). After exposure, the photoresist was developed (step l) using MF702 developer (Shipley, Inc.) and rinsed with DI water. The exposed SiO_2 was then etched with buffered hydrofluoric (BHF) acid solution (step m). The etching was done at both ends of the channel, and the etched region is not shown in Fig. 2 (steps k to o). The remaining photoresist was then striped off with acetone.

If the sacrificial copper layer was etched at this stage, the channel would collapse as soon as the copper layer is etched. This is because of the fact that the structural integrity of a 1×300-μm thin film is not good. Moreover, stiction takes place between the top and bottom of the channel when they are as close as 100 to 200 nm. To avoid this problem, the SiO_2 top layer was bonded with a thick PDMS layer before releasing the very thin copper layer (step n). To bond the PDMS with the SiO_2 layer, the SiO_2 layer was spin-coated with DC Sylgard primer and the PDMS sheet was mounted at the primer treated layer. They were then cured at 80 °C for 6 h.

Finally, the copper was released with electrochemical etching using a $CuSO_4$ bath at a voltage of 6 V (step o). The concentration of $CuSO_4$ was 210 g/l. The setup of electrochemical etching is illustrated in Fig. 4. The sacrificial copper layer was made the anode and a copper plate was used as the cathode. Since the chemical reaction takes place at the cathode and anthode, the sacrificial copper layer lost electrons and dissolved in the solution. The etching time for a 100 nm$\times$300 μm$\times$20 mm channel was about 4 min. However, in traditional wet etching, the exposure to etchant is very small due to the nano- or microscale cross-sectional area (100 to 200 nm$\times$300 μm) of the nanochannel. Thus, the processing time of chemical wet etching is very long. Stern et al.[17] reported that it took 80 h to etch a 100-nm-deep, 5-μm-wide, and 2-mm-long nanochannel using tetra-methyl ammonium hydroxide (TMAH) to selectively etch Si. Note that it would take much longer time if the channel width and length were 300 μm and 20 mm, respectively. On the other hand, in electrochemical etching, the etching time depends on the volume of the sacrificial layer, the concentration of the electrolyte ($CuSO_4$ solution), and the potential across the electrodes. The etching rate of copper electrochemical wet etching is discussed in the next section.

2.2 *Electrochemical Machining*

The dry etching processes for thin-film etching are based on plasma-assisted processes, which include ion etching, plasma etching, and reactive ion etching.[20] Dry-etching techniques are usually used for high-precision etching of thin films involving very small amounts of material removal. However, because of high equipment cost, lack of selectivity, redeposition on the sample, and deposition on the vacuum chamber, concerns arise in terms of the safety, environmental impact, and disposal of the toxic gases. Wet chemical etching involves removal of unwanted material by the exposure of the work piece to an etchant, which is generally aggressive and toxic.[21] Thus, it poses safety and disposal problems, the costs of which often surpass actual etching costs. Electrochemical machining is an alternative wet-etching process. In electrochemical machining, the work piece is used as an anode in an electrolytic cell in which a salt solution is used as an electrolyte. Here the metal removal is controlled by application of an external current. Compared to wet chemical etching, the electrochemical machining process offers better control and flexibility, requires less monitoring and control, and involves minimum safety and environmental concerns.[22,23]

As shown in Fig. 4, in the electrochemical etching of Cu, the chemical reaction takes place at the anode as

$$\mathrm{Cu}-2e\rightarrow\mathrm{Cu}^{2+}, \tag{1}$$

where e is the electron. Here, one reservoir and the majority of the channel were immersed into the solution, while the other reservoir was placed outside the solution. Due to the

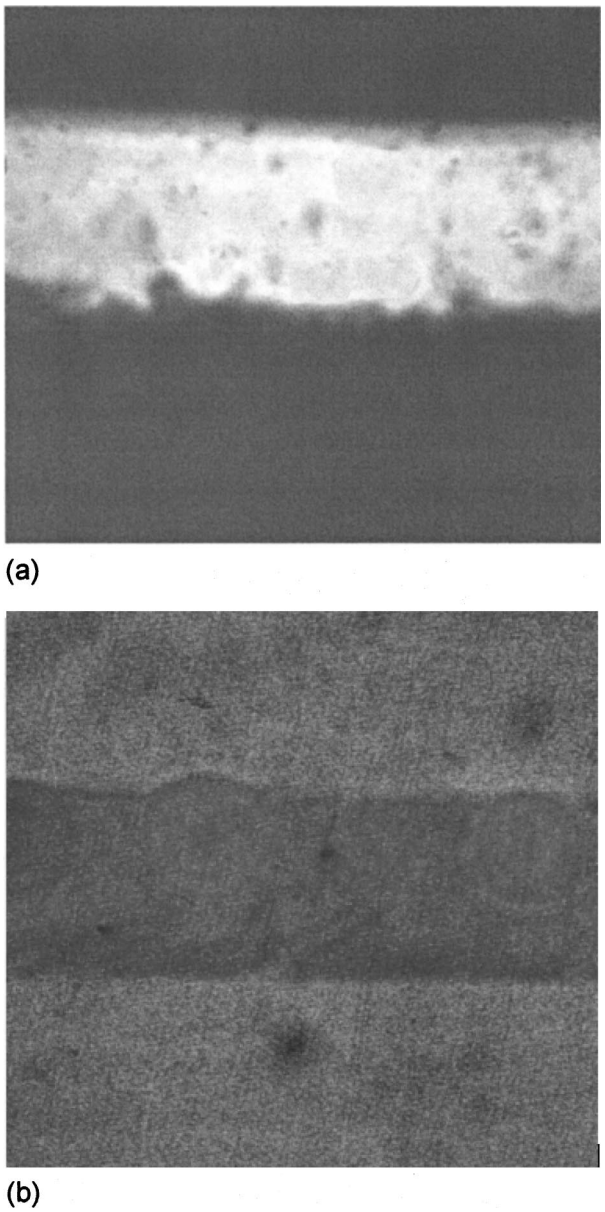

Fig. 5 Optical microscopy image (top view) of a nanochannel (a) before and (b) after releasing the copper layer.

chemical reaction, the Cu sacrificial layer starts coming out from the SiO_2 nanoshell into the solution. The etching front moves up until it reaches the other reservoir outside of the solution, where the chemical reaction on anode stops because of a deficiency of $CuSO_4$ solution. The residual copper outside the solution does not affect the fluidic behavior because the whole channel and part of copper in the reservoir are etched. At the end of the etching process, the current reduces to zero. Figure 5 shows the optical microscopy image (top view) of the nanochannel before and after releasing of the copper layer. It is seen that releasing of Cu is completed, and the channel is clean inside.

The material removal rate in electrochemical machining depends on the specific electrochemical behavior of the metal/electrolyte system, and is determined by the applied current density according to the Faraday law.[24] The material removal rate r, in centimeters per second, is given by

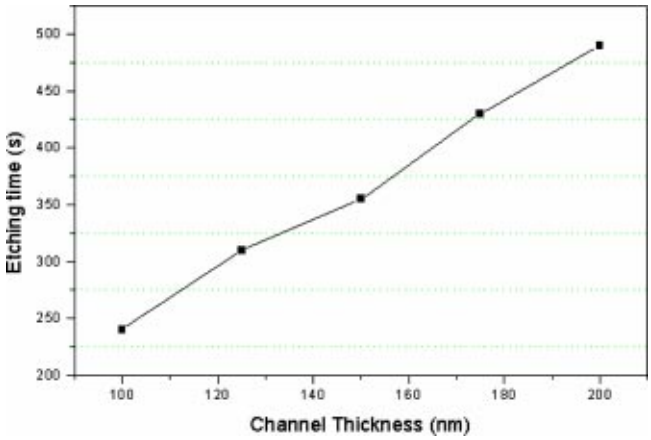

Fig. 6 Variation of electrochemical etching time with different channel thicknesses.

$$r = \frac{IM}{nFA\rho}, \tag{2}$$

where I is the current in amperes, M is the molecular weight of the dissolved material in grams per mole, n is the apparent dissolution valence, F is the Faraday constant ($F = 96485.3383\,\mathrm{C\,mol^{-1}}$), A is the surface area in centimeters square, and ρ is the density in grams per cubic centimeter. The value of n can be determined from weight-loss measurements as

$$n = \frac{IMt}{F\Delta W}, \tag{3}$$

where t is the dissolution time in seconds, and ΔW is the anodic weight loss in grams. With proper considerations of high electrolyte flow velocities and high current efficiency for metal dissolution, extremely high metal removal rates can be obtained. In our experiment, the electric current (I) was 0.065 mA, the density (ρ) of copper was 8.93 g/cm^3, and the molecular weight (M) of the dissolved material (Cu) was 63.5 g/mole. Therefore, from Eq. (3), the apparent dissolution valence (n) is 1.93, which is close to the valence of Cu^{2+}. The dissolution valence (n) depends on the applied voltage/current density, which is essential to determine the operating conditions.[25] The results of experimentally determined dissolution valence for different metal-electrolyte systems under active and passive conditions are summarized in Ref. 24. With the same current (0.065 mA), four other nanochannels of different thicknesses (100 to 200 nm) were released by electrochemical machining. The comparison of etching times for the nanochannels is plotted in Fig. 6. It is seen that the etching time increases linearly with an increase in the channel thickness if the current is kept constant. This can be explained by Eq. (2), which shows the material removal rate (r) decreases with increasing the surface area for a constant current.

Several etching processes in nanochannel fabrication are compared in Table 1. The electrochemical etching pre-

Table 1 Comparison of several etching processes in nanochannel fabrication. Stern et al.[17] have fabricated nano capillary channels utilizing a wet chemical etching technique, and O'Brien et al.[18] made nanofluidic channels based on all-optical lithographic process and reactive ion etching.

	Dry Etching	Wet Etching	
Etching Factors	Reactive Ion Etching[18]	Chemical[17]	Electrochemical (This paper)
Etched material	silicon	silicon	Cu
Etchant/reactive Gas	O_2 and CHF_3	TMAH	$CuSO_4$
Channel geometry (height:width:length)	100 nm:500 nm:20 mm	100 nm:5 μm:2 mm	100 nm:300 μm:20 mm
Etching direction	width	length	length
Etching time	5 min	80 h	4 min
Etching rate	~1000 Å/min	~0.5 μ/min	5 mm/min
Selectivity	moderate	moderate/high	very high
Wall slope control	anisotropic	confined by Si_3N_4	confined by SiO_2
Safety and environmental concerns	moderate/high	high	low
Monitoring and control issues	some	many	few
Cost	high	moderate	low

sented in this paper offers relatively fast etching rate, good selectivity, less safety and environmental concerns, less monitoring and control issues, and low cost.

2.3 *Structural Integrity and Strength of Nanochannel*

2.3.1 *Etching selectivity of Cu and SiO_2*

In traditional chemical etching, the etchants are mostly acidic/alkaline solutions. Therefore, the selectivity of sacrificial layer and channel structural material is very important to avoid thinning of the channel shell, especially when the ratio of channel length to thickness of channel shell are very high, and the etching time is very long. In the experimental work of Stern et al.,[17] the etching selectivity of Si (sacrificial material) and Si_3N_4 (structural material) in TMAH is of the order 10,000 to 1. Hence, they found significant thinning of channel shell (Si_3N_4) after 20 to 80 h of etching. However, in electrochemical machining, the etchants are mostly neutral salt solutions. In this paper, the sacrificial material, Cu, works as the anode, while the shell material, SiO_2, is a very good insulator. The electrolyte used in this paper is neutral $CuSO_4$ solution. Consequently there was no chemical reaction between the electrolyte and the SiO_2 shell structure. Therefore, the selectivity of Cu and SiO_2 in electrochemical etching is infinity (theoretically) to prevent any thinning of channel shell.

Here, the surface roughness of the nanochannel is determined by the roughness of the sacrificial copper film. In the past, the surface roughness of metallic thin films was studied as a function of substrate materials, substrate conditions, and the preparation method[26,27] (evaporation, sputtering, speed, angle). It is reported[28] that the surface roughness obtained from metallic thin film sputtering can achieve 4 nm when sputtering thickness is 1 μm. Hence, the surface roughness of the nanochannel is very smooth.

2.3.2 *Collapse*

The strength of the channel depends on the channel width, since the thickness of channel shell is of the order 1 to 5 μm. Stern et al.[17] found that nanochannel shells with widths greater than 30 μm crack, peel, and collapse as soon as the sacrificial layer (amorphous Si) is removed; after 20 h, 20-μm-wide channels collapse; and at times longer than 50 h, 10-μm-wide channels, and eventually even 5-μm-wide channels collapse. The collapse is due to the deflection of the channel shell and thermal stress developed during the deposition at a high temperature. In this paper, this problem is addressed by bonding the SiO_2 channel with the PDMS material before electrochemical release of the sacrificial layer. The channel shell is supported by the PDMS material during the releasing process. Figure 7 shows atomic force microscopy (AFM) images taken on the cross section of a nanochannel after 1 week. It is seen that there is no crack or collapse on the corner and at the middle of the channel. The structural integrity of the channel is further enhanced with deposition of the channel shell (SiO_2) directly on the SiO_2 substrate. Therefore, the bonding of channel to substrate is strong, and the channel is expected to sustain the very large pressure required to fill the nanofluidic channel. Figure 8 shows the scanning electron microscopy images obtained across the nanochannel. A fairly uniform 150-nm-deep nanochannel is obtained. In Fig. 8, only the edge of the channel is shown since the width of the channel is 300 μm, which is much longer than the height of the channel.

2.4 *Fabrication of Microchannel*

Polymeric PDMS was used for fabrication of the microchannel. PDMS basically consists of a base elastomer (vinyl group and platinum catalyst in GE RTV 615) and a curing agent (cross linker Si-H). It is transparent and permeable to a variety of liquids, carries a low surface energy,

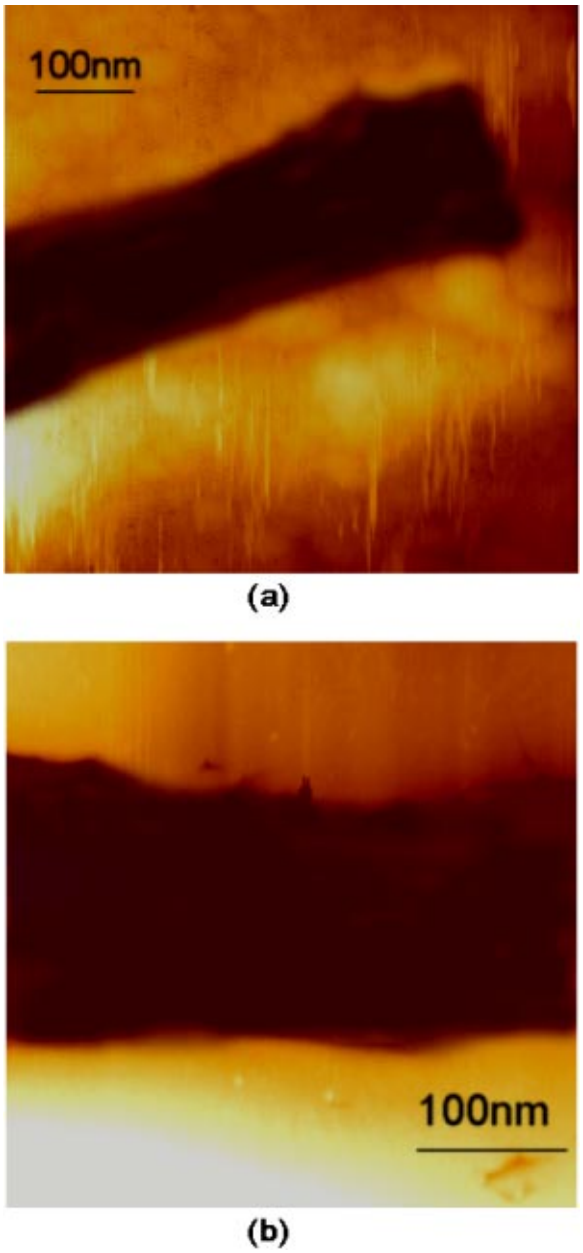

Fig. 7 AFM images of the cross-sectional view of a nanochannel (width=300 μm and height=150 nm) (a) near the edge of the channel and (b) at the middle of the channel.

and acquires negative charges on the surface when it comes in contact with weak electrolytes such as DI water at a pH of 5 to 6.

Microfluidic flow channels and reservoirs were formed on PDMS utilizing recently invented soft lithography techniques. Soft lithography technique offers certain advantages over both bulk and surface micromachining in which an elastomer is patterned by curing on a micropatterned mold. Some of the positive aspects of soft lithography are rapid prototyping, shorter turn out time, mass scale production, and cheaper device cost.[29] Soft lithography can also be used for multilayer bonding of two different kinds of materials, such as glass and PDMS or acrylic and PDMS (Ref. 29).

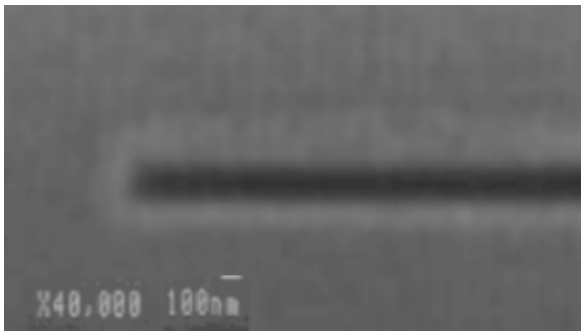

Fig. 8 Cross-sectional view of a nanochannel obtained from scanning electron microscopy.

Figure 9 shows the microfabrication schemes on a glass microslide. The glass plate was cleaned with acetone, DI water, and isopropyl alcohol (IPA) and dried with compressed air. Photoresist (AZ 4620), of the order of the channel thickness, was then spin-coated on the planar glass substrate. The thickness of the photoresist can be varied from 2 to 10 μm by changing the spin rate and time. For example, the spincoater (Model P6204-A) was set at 3000 rpm for 30 s to form a 3-μm-deep channel. This was followed by the softbaking of the photoresist on a hotplate (Model 04744 Series Digital Hot Plate/Stirrer) for 5 min at 70 °C. The next step was to etch a channel manifold on the photoresist using a protective mask. A mask, which can be made of a high-resolution transparency film printed to scale, was held right over the photoresist using a mask aligner (Hybralign Series 500) and then a near-UV beam (300 to 350 nm) was illuminated for 60 s to make a positively etched channel pattern. The photoresist was then vacuum dried for 1 h, and the excess photoresist was carefully dissolved from the glass substrate and washed repeatedly with developing fluid. In this case, the developer fluid was prepared by mixing the DI water with the developer (AZ 400) at a ratio of 4:1. At the end of the photolithography, the photoresist was rinsed with DI water and blow dried with compressed air.

Once the glass microslide had the positive pattern of the sample channel, two capillaries were attached at the reservoirs locations. Next, two components of PDMS (base and curing agent) were mixed, degassed in a vacuum desiccator for 1 h, and the liquid polymer was then poured onto the positively patterned mold and let it cure at 80 °C for 6 h. At the end of the curing process, the PDMS layer was peeled off from the glass substrate, and we submerged the sample into acetone for 2 h. Finally, the PDMS layer was rinsed with DI water and IPA and blow dried with compressed air. This PDMS layer was used as the top surface for the integrated hybrid micro/nanofluidic channel network.

Figure 10 shows a cross-sectional view of the PDMS microchannel obtained from a profilometer (SPN Technology Inc.). Here, the channel height is presented in terms of angstroms and the channel width is illustrated in millimeters. A fairly rectangularly shaped microchannel was obtained from the soft lithography techniques. From Fig. 10, it is clear that the surface roughness of the PDMS microchannel is less than 150 nm. The channel roughness mainly originated from the surface coarseness of the commercially available glass slide used in the photolithography technique. However, the channel surface roughness can be re-

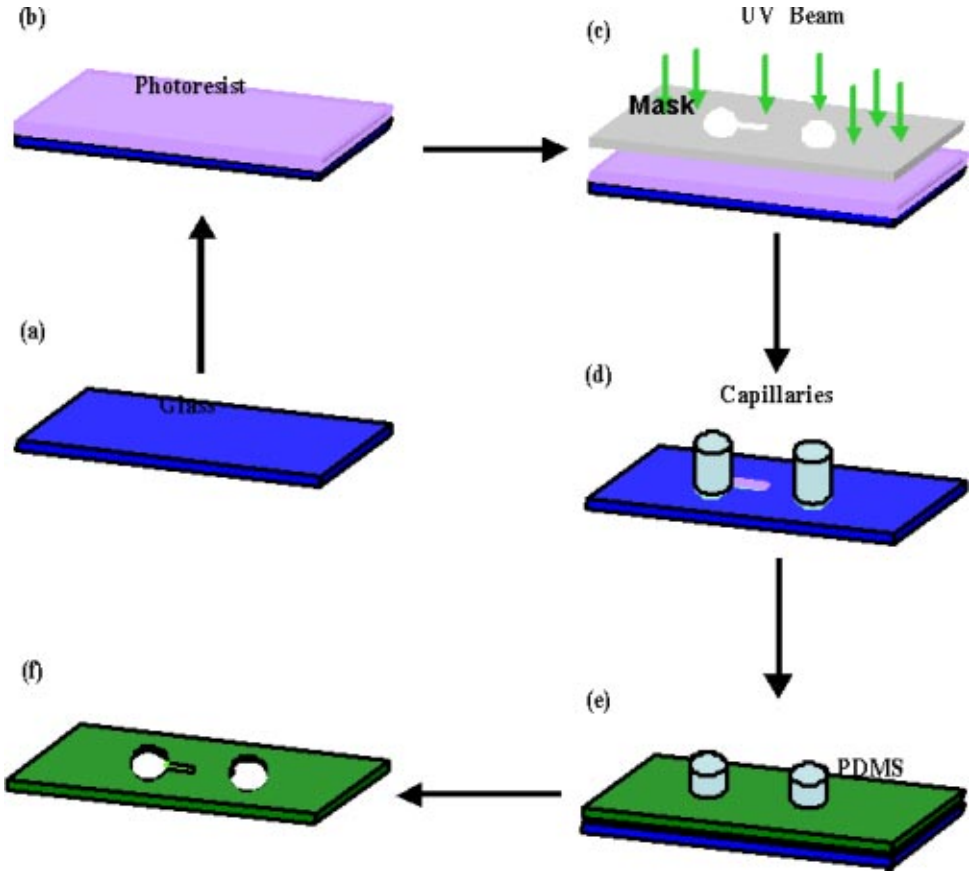

Fig. 9 Schematic view of the soft lithography technique to form a microchannel on PDMS.

duced significantly by using a high-quality silicon wafer instead of commercial glass during photolithography stages.

2.5 *Integration of Nanochannel with a Micro/Mesofluidic System*

In this section, we describe the integration techniques used to form the hybrid micro-nanofluidic systems. First, we fabricated a nanochannel structure on a silicon wafer using the surface nanomachining techniques, which was filled with copper [steps shown in Figs. 2(a) to 2(m)]. Then the top layer of our integrated device was fabricated using soft lithography techniques. This PDMS layer contains reservoirs (sample and waste) and a discontinuous microfluidic channel. Once both upper and lower parts were ready, they were placed on oxygen plasma for a couple of minutes. The function of the plasma cleaner is not only to remove any dust/organic particles, but also to activate the surfaces of PDMS and SiO_2 for chemical bonding. Next, the top and bottom layers were aligned under an optical microscope and cured on a hot plate for 6 h at 80 °C. At the end of the curing process, the top and bottom layers were chemically bonded to each other to create an assembly like that of Fig. 11. Hence, the interface has a strength identical to that of

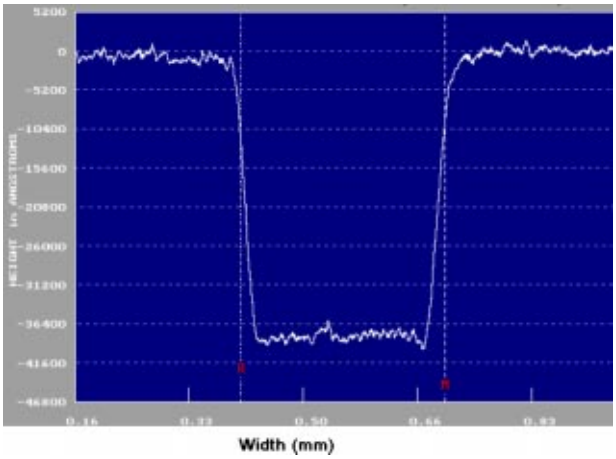

Fig. 10 Cross-sectional view of a PDMS microchannel obtained from a profilometer.

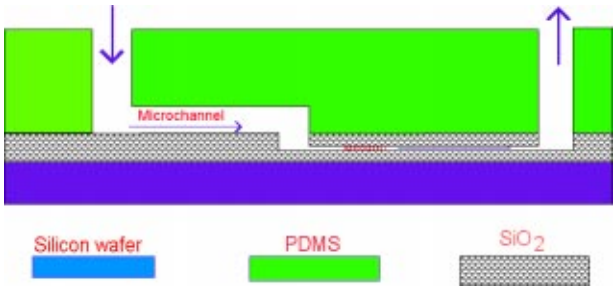

Fig. 11 Integration of nanochannel in micro/mesofluidic systems.

the bulk elastomer to prevent any leakage of liquid from the system. Next, electrochemical etching was applied to release the copper from the SiO_2 shell by applying an electric current through the inlet reservoir.

3 Conclusions

We developed a hybrid micro-nanofluidic channel networks, which could be used in various bioanalytical operations. PDMS and silicon dioxide were used as the microchannel and nanochannel materials, respectively. Our nanofabrication techniques consist of surface machining, wafer bonding, and electrochemical etching, while soft lithography is used to form the microfluidic channels and reservoirs. The novel nanofabrication techniques presented in this paper offer a number of important advantages over existing techniques.

1. The mechanical strength of the nanochannel is very strong because SiO_2 is deposited on SiO_2, and the nanochannel could sustain the very large pressure that must be applied to fill the nanochannel.
2. The nanochannel manifold is created by sputtering sacrificial copper film on the SiO_2 layer. Hence, the surface roughness of the nanochannel was very smooth, which is extremely important in the nanofluidic operations.
3. PDMS material is bonded with a SiO_2 nanoshell before releasing the sacrificial layer. This increases the structural integrity and makes it convenient for integration of nanochannel with PDMS micro/mesochannel.
4. Since the opening of the channel is of micro/nanosize, the sacrificial layer is released by electrochemical etching. While a traditional releasing method such as wet chemical etching is very time consuming, the electrochemical machining provides a relatively fast etching rate, good selectivity, fewer safety and environmental concerns, fewer monitoring and control issues, and low cost.

Acknowledgments

The authors thank Mr. Keisuke Horiuchi for his valuable help in the microfabrication. This investigation was supported in part by the Washington State University Office of Research and in part by the National Science Foundation under Grant No. CTS-0300802.

References

1. R. Qiao and N. R. Aluru, ''Transient analysis of electro-osmotic transport by a reduced-order modelling approach,'' *Int. J. Numer. Methods Eng.* **56(7)**, 1023–1050 (2003).
2. A. Acrivos, B. Khusid, J. Koplik, and G. Drazer, ''Squeezing flow of particles and large molecules suspended in a liquid through nanochannels,'' in *Proc. 2002 Int. Conf. on Modeling and Simulation of Microsystems, NanoTech 2002*, pp. 66–67, Nano Science and Technology Institute (2002).
3. V. M. Ugaz, R. S. Lin, N. Srivastava, D. T. Burke, and M. A. Burns, ''A versatile microfabricated platform for electrophoresis of double- and single-stranded DNA,'' *Electrophoresis* **24**, 151–157 (2003).
4. F. Raisi, P. Belgrader, D. A. Borkholder, A. E. Herr, G. J. Kintz, F. Pourhamadi, M. T. Taylor, and M. A. Northrup, ''Microchip isoelectric focusing using a miniature scanning detection system,'' *Electrophoresis* **22(11)**, 2291–2295 (2001).
5. B. B. Haab and R. A. Mathies, ''Single molecule detection of DNA separations in microfabricated capillary electrophoresis chips employing focused molecular streams,'' *Anal. Chem.* **71(22)**, 5137–5145 (1999).
6. J. Y. Han and H. G. Craighead, ''Characterization and optimization of an entropic trap for DNA separation,'' *Anal. Chem.* **74(2)**, 394–401 (2002).
7. H. Cao, Z. N. Yu, J. Wang, J. O. Tegenfeldt, R. H. Austin, E. Chen, W. Wu, and S. Y. Chou, ''Fabrication of 10 nm enclosed nanofluidic channels,'' *Appl. Phys. Lett.* **81(1)**, 174–176 (2002).
8. H. G. Craighead, ''Nanoelectromechanical systems,'' *Science* **290**, 1532–1535 (2000).
9. C. L. Rice and R. Whitehead, ''Electro kinetic flow in a narrow cylindrical capillary,'' *J. Phys. Chem.* **69**, 4017–4023 (1965).
10. X. J. Fan, N. Phan-Thien, N. T. Yong, and X. Diao, ''Molecular dynamics simulation of a liquid in a complex nano channel flow,'' *Phys. Fluids* **14(3)**, 1146–1153 (2002).
11. C. K. Harnett, G. W. Coates, and H. G. Craighead, ''Heat-depolymerizable polycarbonates as electron beam patternable sacrificial layers for nanofluidics,'' *J. Vac. Sci. Technol. B* **19(6)**, 2842–2845 (2001).
12. A. Hibara, T. Saito, H. B. Kim, M. Tokeshi, T. Ooi, M. Nakao, and T. Kitamori, ''Nanochannels on a fused-silica microchip and liquid properties investigation by time-resolved fluorescence measurements,'' *Anal. Chem.* **74(24)**, 6170–6176 (2002).
13. H. Cao, J. O. Tegenfeldt, R. H. Austin, and S. Y. Chou, ''Gradient nanostructures for interfacing microfluidics and nanofluidics,'' *Appl. Phys. Lett.* **81(16)**, 3058–3060 (2002).
14. V. Studer, A. Pepin, and Y. Chen, ''Nanoembossing of thermoplastic polymers for microfluidic applications,'' *Appl. Phys. Lett.* **80(19)**, 3614–3616 (2002).
15. S. Y. Chou, P. R. Krauss, and P. J. Renstrom, ''Imprint of sub-25 nm vias and trenches in polymers,'' *Appl. Phys. Lett.* **67(21)**, 3114–3116 (1995).
16. M. Colburn, A. Grot, B. J. Choi, M. Amistoso, T. Bailey, S. V. Sreenivasan, J. G. Ekerdt, and C. G. Willson, ''Patterning non-flat substrates with a low pressure, room temperature, imprint lithography process,'' *J. Vac. Sci. Technol. B* **19(6)**, 2162–2172 (2001).
17. M. B. Stern, M. W. Geis, and J. E. Curtin, ''Nanochannel fabrication for chemical sensors,'' *J. Vac. Sci. Technol. B* **15(6)**, 2887–2891 (1997).
18. M. J. O'Brien, P. Bisong, L. K. Ista, E. M. Rabinovich, A. L. Garcia, S. S. Sibbett, G. P. Lopez, and S. R. J. Brueck, ''Fabrication of an integrated nanofluidic chip using interferometric lithography,'' *J. Vac. Sci. Technol. B* **21(6)**, 2941–2945 (2003).
19. L. J. Guo, X. Cheng, and C. F. Chou, ''Fabrication of size-controllable nanofluidic channels by nanoimprinting and its application for DNA stretching,'' *Nano Lett.* **4(1)**, 69–73 (2004).
20. J. L. Vossen and W. Kern, *Thin Film Processes*, Academic, New York (1991).
21. O. A. Moreno, R. C. McHatten, R. S. Paonessa, and R. H. Magnuson, ''Etching of metals by wet processes in electronic packaging,'' in *Principles of Electronic Packaging*, D. P. Seraphim, R. C. Lasky, and C. Y. Li, Eds., McGraw-Hill, New York (1989).
22. M. Datta, ''Electrochemical Micromachining,'' in *Electrochemical Technology: Innovations and New Developments*, N. Masuko, T. Osaka, and Y. Ito, Eds., Kodansha/Gordon and Breach, Tokyo (1996).
23. M. Datta, ''A 'greener' method of producing metal parts,'' *Interface (USA)* **4(2)**, 32–35 (1995).
24. M. Datta, ''Anodic dissolution of metals at high rates,'' *IBM J. Res. Dev.* **37(2)**, 207–226 (1993).
25. M. Datta, ''Microfabrication by electrochemical metal removal,'' *IBM J. Res. Dev.* **42(5)**, 655–670 (1998).
26. E. Anguiano, A. I. Oliva, and M. Aguilar, ''Surface texture parameters as a tool to measure image quality in scanning probe microscope,'' *Ultramicroscopy* **77(3–4)**, 195–205 (1999).
27. M. Aguilar, A. I. Oliva, and E. Anguiano, ''The importance of imaging conditions in scanning tunneling microscopy for the determination of surface texture and roughness,'' *Surf. Sci.* **420(2–3)**, 275–284 (1999).
28. *MEMS exchange*: http://www.mems-exchange.org/catalog/deposition/.
29. M. A. Unger, H. P. Chou, T. Thorsen, A. Scherer, and S. R. Quake, ''Monolithic microfabricated valves and pumps by multilayer soft lithography,'' *Science* **288**, 113–116 (2000).

Gary J. Cheng is an assistant professor at the School of Mechanical and Materials Engineering, Washington State University. He received his PhD from the Department of Mechanical Engineering, Columbia University, in 2002. His research areas are non-traditional manufacturing, laser materials processing, and design and fabrication for MEMS.

Daniel Pirzada received his BSc in Chemistry from Punjab University, Lahore. He received his Masters in Metallurgical Engineering and Mechanical Engineering from the University of Idaho, Moscow, Idaho. Presently he is pursuing a PhD in Mechanical Engineering at Washington State University, Pullman, Washington.

Prashanta Dutta received his BSc and MSc Engineering degrees in Mechanical Engineering from Bangladesh University of Engineering and Technology, Dhaka, Bangladesh in 1993 and 1995, respectively. He received his MSME degree from the University of South Carolina, Columbia, South Carolina, in 1997 and his PhD degree from Texas A&M University, College Station, Texas, in 2001. He has been working as an assistant professor in the School of Mechanical and Materials Engineering at Washington State University since August 2001. His current research focus is on micro/nano-scale transport modeling, fabrication of micro/nanofluidic chips, microscale flow visualization, and electrophoretic separation and purification of proteins and DNAs in microchips.